



Shahid Chamran
University of Ahvaz

Journal of Applied and Computational Mechanics



Research Paper

Stability Analysis of Casson Nanofluid Flow over an Extending/Contracting Wedge and Stagnation Point

H. Thameem Basha^{id}, R. Sivaraj^{id}

Department of Mathematics, School of Advanced Sciences, Vellore Institute of Technology, Vellore-632014, India, Emails: basha.thameem666@gmail.com, sivaraj.kpm@gmail.com

Received February 13 2020; Revised May 05 2020; Accepted for publication May 10 2020.

Corresponding author: R. Sivaraj (sivaraj.kpm@gmail.com)

© 2021 Published by Shahid Chamran University of Ahvaz

Abstract. This numerical study is conducted to scrutinize the dual solutions and stability analysis of the flow of Casson nanofluid past a permeable extending/contracting wedge and stagnation point. Momentum, heat and mass transfer behaviors of the Casson nanofluid have been modeled with the use of the Buongiorno nanofluid model. Suitable self-similarity variables are employed to convert the fluid transport equations into ordinary differential equations and the bvp4c MATLAB solver is used to solve the equations. The impacts of active parameters on fluid transport properties are illustrated graphically. The outcomes of the present analysis reveal that the influence of Casson fluid parameter on velocity and temperature distributions obtained from the first and second solutions exhibit the opposite natures. From the stability analysis, it is found that the thermophoresis and Brownian motion effects acquire the same critical point value on Nusselt number. The temperature distribution of the Casson nanofluid is higher over the wedge than stagnation point. The two solutions are found for the limited range of extending/contracting parameter. The detailed stability test is carried out to determine which of the two solutions is physically realizable and stable.

Keywords: Casson nanofluid, Dual solutions, Stability test, Falkner-Skan flow, Wedge/stagnation point.

1. Introduction

Non-Newtonian fluids are the fluids which have viscosity shear-dependence along with shear-thinning/shear-thickening characteristics. These fluids have numerous industrial applications, like petroleum production, chemical process industries, plastic polymers, food preservation techniques, cosmetic products, and manufacture of optical fibers. The non-Newtonian fluids have complex rheological characteristics, so the flow properties of such fluids cannot be elucidated by the Navier-Stokes equations. As a result, Casson fluid, Maxwell fluid, Williamson fluid, Cross fluid, Walter's B-fluid and Carreau fluid models have been proposed by various researchers. Transport characteristics of various non-Newtonian fluid models were investigated by several researchers [1-5]. Casson fluid is one of the subclasses of non-Newtonian fluids which was coined by Casson [6]. It is seen that this fluid model has a high viscosity and low viscosity when β (Casson fluid parameter) $\rightarrow 0$ and $\beta \rightarrow \infty$, respectively. It is also noticed that this model is expressing the shear-thinning behavior in nature which manifests liquid characteristics when shear stress is higher than the yield stress while it can express the solid characteristics when shear stress is lower than the yield stress. The Casson fluid model has received notable attention due to its significance in characterizing the rheological behavior of human blood, jelly, honey, and tomato sauce. Mythili and Sivaraj [7] have scrutinized the time-dependent Casson fluid flow over two different geometries by means of uneven energy gain/loss and have found that Casson fluid parameter uplifts the fluid velocity. Raju et al. [8] have employed Runge-Kutta method to explore the heat and mass transfer characteristics of Casson nanofluid by considering suction/injection and have noticed that higher values of Casson fluid parameter tend to decline the fluid temperature. Hamid et al. [9] have addressed the stability and dual solutions of Casson fluid in an expanding/contracting sheet with linear radiation and have observed that higher values of expanding/contracting parameter cause to enhance the skin friction of Casson fluid for the first solution. Some recent studies on Casson fluid are shown in Refs. [10-12].

One of the prime issues in electronic equipment, power generation, automobile industries and industrial processes is to enhance the heat transfer rate. The poor thermal properties of regular heat dissipation fluids are not sufficient for today's needs. Choi et al. [13] have proposed a technique to increase the heat transfer rate in fluids by suspending one to hundred nanometers sized metal oxide/carbon/metal particles in regular fluids and the fluids obtained in this way are called nanofluids. The nanofluids have massive use in numerous fields like solar energy [14], biomedical [15], drug targeting, cancer treatment, cooling the engine radiators [16], food technology [17], biomass and geothermal. To investigate the characteristics of nanofluids, researchers have presented various nanofluid models like single-phase and two-phase models. In the single-phase model, researchers are examining the fluid transport characteristics of nanofluid using the base fluid and nanoparticles thermophysical properties. Abbasi et al. [18] have illustrated the entropy generation and heat transfer behavior of water-based copper nanofluid flow in the presence of Hall current and Joule heating and have seen that the total entropy generation rises by increasing nanoparticle volume fraction. Abbasi et al. [19] have utilized the homotopy perturbation method to examine the peristaltic



transport of water-based copper nanofluid in a symmetric channel with the effects of variable viscosity and Hall current and have noted that fluid temperature decline with an increment in viscosity parameter. The Buongiorno (two phase) model is one of the notable models in nanofluid which is utilized by several researchers to explore the transport characteristics of nanofluid. In Buongiorno [20] model, the fluid transport characteristics are investigated by means of thermophoretic diffusivity and Brownian movement. Basha et al. [21] have performed a numerical study on the free convection flow of nanofluid over two different geometries with the influence of slip mechanisms (thermophoresis and Brownian motion) and have reported that the slip mechanisms augment the nanofluid temperature. Abbasi et al. [22] have scrutinized the influences of Hall current and Joule heating on peristaltic nanofluid flow by utilizing Buongiorno nanofluid model and have noted that fluid concentration upsurges with the increment of thermophoresis. Waqas et al. [23] have employed a Buongiorno nanofluid model to analyze the radiation impact on hydromagnetic Jeffrey nanofluid flow and have found that the higher thermophoresis and Brownian motion enhance the Jeffrey fluid the temperature. Riaz et al. [24] have utilized a Buongiorno nanofluid model to investigate the entropy generation and fluid transport properties of peristaltic viscoelastic nanofluid flow over a two asymmetric annuli and have observed that the Grashof number elevates the pumping rate. Basha et al. [25] numerically explored the variable fluid properties of Williamson nanofluid flow over three different geometries by means of thermophoresis and Brownian motion. Some recent investigations on the two-phase nanofluid model have shown in references [26-30].

In recent time, researchers and engineers are interested in scrutinizing the fluid flow over a stretching/shrinking sheet owing to its notable utilization in various industrial processes like nuclear reactor cooling, wire drawing, glass-fiber production, plastic films drawing, extraction of polymer, crystal growing, hot rolling and aerodynamics. Bachok et al. [31] have reported on the dual natures of viscous fluids over a melting expanding/contracting sheet with Lorentz force and have shown that the Lorentz force diminishes the fluid velocity and temperature for the upper solution. Alam et al. [32] have explained the impacts of variable viscosity, Prandtl number and Schmidt number on time-dependent viscous fluid flow over a permeable expanding/contracting wedge. Pop et al. [33] have performed a numerical study with the aim to express the heat transfer characteristics of three different nanoparticles namely Cu, Al₂O₃ and TiO₂ and have shown that Cu nanoparticles have higher heat transfer rate than the other two nanoparticles. Dogonchi and Ganji [34] have utilized the Duan-Rach Approach to explore the fluid transport characteristics of Cu/water nanofluid in a stretching/shrinking channel. Hamid et al. [35] have employed the Williamson fluid model to investigate the heat transfer characteristics over a permeable expanding/contracting sheet and have found that both solutions lessen the Williamson fluid velocity for larger values of Weissenberg number. Hashim et al. [36] have presented an in-depth investigation on unsteady Carreau nanofluid flow over an expanding/contracting disk in the presence of non-linear radiation and have concluded that the upper and lower solutions have an opposite natures in Carreau nanofluid velocity for uplifting the suction/injection parameter. Usman et al. [37] have carried out a numerical study to determine the stability test and dual natures of Cu-water based nanofluid with velocity and thermal slips and have pointed out that the first solution is stable but the second solution is not stable. Several researchers have explored the two solutions and stability test in the presence of extending/contracting surface over different geometries [38-40].

The prime intention of the present model is to exhibit the dual solutions and stability analysis of Casson nanofluid flow over two different geometries in the presence of slip mechanisms. The non-homogeneous equilibrium model is employed to model the present problem. The self-similarity variables have been obtained to consider the value of Prandtl number for any fluid. It is observed from a significant analysis of the current literature that no effort has been made to explore the dual natures and stability analysis of the forced convective flow of Casson nanofluid over two different geometries in the presence of thermophoresis and Brownian motion. According to the consequence of this kind of problems, the current effort aims to address the following research questions:

- I. How many solutions occur when extending/contracting two geometries?
- II. In the obtained solutions, which solution is physically realizable and stable?
- III. What is the variation in the heat transfer rate of Casson nanofluid flow over two different geometries?
- IV. What are the impacts of thermophoresis and Brownian motion effects on the heat and mass transfer rates?

The system of fluid transport equations is solved numerically by using bvp4c collocation formula in MATLAB. It is noticed that two solutions exist for expanding/contracting wedge as well as stagnation point. A stability test is performed to verify the stability of two solutions. The impacts of the active parameters are illustrated via 2-dimensional plots and contour plots.

2. Mathematical Formulation

The schematic view of two different geometries is manifested in Fig. 1. $u_\infty = bx^m$ is the free stream velocity where b is the constant. The Hartree pressure gradient m can be expressed as $1/[(2/\beta_1) - 1]$. The values 0.5 and 1 of β_1 represent the Casson nanofluid flow over the wedge and stagnation point, respectively. The constant temperature (T_w) and concentration (C_w) of the wall is presumed to be greater than the ambient temperature (T_∞) and ambient concentration (C_∞), respectively. The Falkner-Skan, incompressible, time-independent, forced convective, laminar flow of Casson nanofluid is considered. The governing equations are expressed by employing a two-phase nanofluid model. The wedge and stagnation point surface are permeable and experience the extending/contracting behavior. Based on these assumptions, the flow of Casson nanofluid is governed by the following equations [7, 8, 21, 25 and 35]:

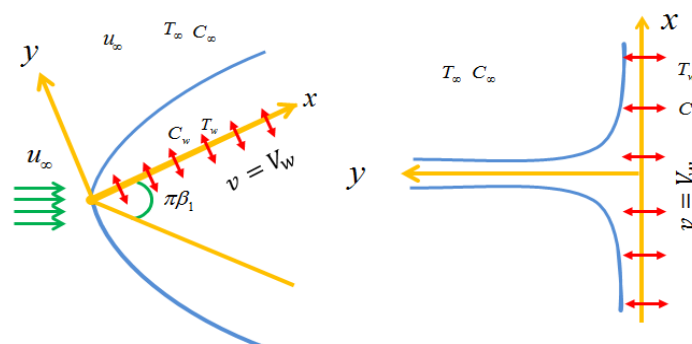


Fig. 1. Physical configuration of the flow geometry



$$\frac{\partial u}{\partial x} + \frac{\partial v}{\partial y} = 0, \tag{1}$$

$$\rho_f \left(u \frac{\partial u}{\partial x} + v \frac{\partial u}{\partial y} \right) = \rho_f u_\infty \frac{du_\infty}{dx} + \mu_f \left(1 + \frac{1}{\beta_T} \right) \frac{\partial^2 u}{\partial y^2} \tag{2}$$

$$(\rho C_p)_f \left(u \frac{\partial T}{\partial x} + v \frac{\partial T}{\partial y} \right) = k_f \frac{\partial^2 T}{\partial y^2} + (\rho C_p)_p \left[D_B \frac{\partial T}{\partial y} \frac{\partial C}{\partial y} + \frac{D_T}{T_\infty} \left(\frac{\partial T}{\partial y} \right)^2 \right] \tag{3}$$

$$u \frac{\partial C}{\partial x} + v \frac{\partial C}{\partial y} = D_B \frac{\partial^2 C}{\partial y^2} + \frac{D_T}{T_\infty} \frac{\partial^2 T}{\partial y^2}. \tag{4}$$

The boundary conditions are [8, 25 and 35]:

$$\begin{aligned} u = \lambda_T u_\infty, \quad v = V_w, \quad T = T_w, \quad C = C_w \quad \text{at} \quad y = 0, \\ u \rightarrow u_\infty, \quad T \rightarrow T_\infty, \quad C \rightarrow C_\infty \quad \text{as} \quad y \rightarrow \infty. \end{aligned} \tag{5}$$

where u and v represent the velocity components along the x and y -directions, $\nu_f = \mu_f / \rho_f$ is the kinematic viscosity, μ_f is the dynamic viscosity, ρ_f is the density of fluid, β_T is the Casson fluid parameter, $\alpha^* = k_f / (\rho C_p)_f$ is the thermal diffusivity, k_f is the fluid thermal conductivity, C_p is the specific heat capacity, $\tau = (\rho C_p)_p / (\rho C_p)_f$ is the ratio between particle and base fluid, T is the fluid temperature, D_B is the Brownian diffusion, D_T is the thermophoretic diffusion and C is the concentration. Suitable self-similarity variables are expressed as follows

$$\left. \begin{aligned} \eta &= \lambda \left(\frac{y}{x} \right), \\ f(\eta) &= \frac{\psi(x, y)}{\lambda \alpha^*}, \\ u &= \frac{b x^m f'(\eta)}{(1 + Pr)^{2n}}, \\ v &= -\lambda \left(\frac{\alpha^*}{x} \right) \left[\left(\frac{m+1}{2} \right) f(\eta) + \left(\frac{m-1}{2} \right) \eta f'(\eta) \right], \\ V_w &= -\left(\frac{\alpha^*}{x} \right) \lambda f_w \left(\frac{m+1}{2} \right), \\ T &= T_\infty + \theta(\eta)(T_w - T_\infty), \quad C = C_\infty + \chi(\eta)(C_w - C_\infty). \end{aligned} \right\} \tag{6}$$

By implementing the above variables, Eqns. (2) - (4) are converted to

$$Pr f''' \left(1 + \frac{1}{\beta_T} \right) + \left(\frac{m+1}{2} \right) f f'' + m(1 + Pr)^{4n} - m(f')^2 = 0, \tag{7}$$

$$\theta'' + \left(\frac{m+1}{2} \right) f \theta' + Pr N_b \theta' \chi' + Pr N_T (\theta')^2 = 0, \tag{8}$$

$$\chi'' + \left(\frac{m+1}{2} \right) f \chi' \frac{Sc}{Pr} + \frac{N_T}{N_b} \theta'' = 0. \tag{9}$$

Along with the transformed boundary conditions

$$\begin{aligned} f(\eta) = f_w, \quad f'(\eta) = \lambda_T (1 + Pr)^{2n}, \quad \theta(\eta) = 1, \quad \chi(\eta) = 1 \quad \text{at} \quad \eta = 0, \\ f'(\eta) \rightarrow (1 + Pr)^{2n}, \quad \theta(\eta) \rightarrow 0, \quad \chi(\eta) \rightarrow 0 \quad \text{as} \quad \eta \rightarrow \infty. \end{aligned} \tag{10}$$

where f_w is the suction/injection parameter, $Pr = \nu_f / \alpha^*$ is the Prandtl number, $N_b = \tau D_B (C_w - C_\infty) / \nu_f$ is the Brownian movement parameter $N_T = \tau D_T (T_w - T_\infty) / T_\infty \nu_f$ is the thermophoresis parameter and $Sc = \nu_f / D_B$ is the Schmidt number. Lin and Lin [41] have introduced a parameter $\lambda = \sqrt{Re} \delta$ which can fit for the value of any fluid Prandtl number (Pr), $Re = u_\infty x \nu^{-1}$ is Reynolds number, $\delta = (1 + Pr)^{-n} \sqrt{Pr}$, $n = 1/6$ for plate ($\beta_1 = 0$), wedge ($\beta_1 = 0.5$), and stagnation of flat plate ($\beta_1 = 1$). At the wall, the dimensionless forms of skin friction factor (C_f^*), heat transfer rate (Nu^*) and mass transfer rate (Sh^*) are expressed as follows:

$$\left. \begin{aligned} C_f^* Re^{1/2} &= \left(1 + \frac{1}{\beta_T} \right) \frac{2 f''(0) \sqrt{Pr}}{\sqrt{1 + Pr}}, \\ Nu^* Re^{1/2} \delta^{-1} &= -\theta'(0), \quad Sh^* Re^{1/2} \delta^{-1} = -\chi'(0). \end{aligned} \right\} \tag{11}$$



3. Stability Test

The stability test is carried out by following the study of Makinde [38 and 42] and results manifest that the second solutions are unstable, whereas the first solutions are stable. To perform a stability test, we have proposed a dimensionless time-dependent variable τ^* to model the problem. Thus we have

$$\rho_f \left(\frac{\partial u}{\partial t} + u \frac{\partial u}{\partial x} + v \frac{\partial u}{\partial y} \right) = \rho_f u_\infty \frac{du_\infty}{dx} + \mu_f \left(1 + \frac{1}{\beta_\tau} \right) \frac{\partial^2 u}{\partial y^2}, \tag{12}$$

$$(\rho C_p)_f \left(\frac{\partial T}{\partial t} + u \frac{\partial T}{\partial x} + v \frac{\partial T}{\partial y} \right) = k_f \frac{\partial^2 T}{\partial y^2} + (\rho C_p)_p \left[D_b \frac{\partial T}{\partial y} \frac{\partial C}{\partial y} + \frac{D_T}{T_\infty} \left(\frac{\partial T}{\partial y} \right)^2 \right], \tag{13}$$

$$\frac{\partial C}{\partial t} + u \frac{\partial C}{\partial x} + v \frac{\partial C}{\partial y} = D_b \frac{\partial^2 C}{\partial y^2} + \frac{D_T}{T_\infty} \frac{\partial^2 T}{\partial y^2}. \tag{14}$$

and the new self-similarity variables are as follows:

$$\left. \begin{aligned} \eta &= \lambda \left(\frac{y}{x} \right), \\ f(\eta, \tau^*) &= \frac{\psi(x, y)}{\lambda \alpha^*}, \\ u &= \frac{bx^m}{(1 + Pr)^{2n}} \left(\frac{\partial f(\eta, \tau^*)}{\partial \eta} \right), \\ v &= -\lambda \left(\frac{\alpha^*}{x} \right) \left[f(\eta, \tau^*) \frac{m+1}{2} + \eta \frac{\partial f(\eta, \tau^*)}{\partial \eta} \frac{m-1}{2} + \tau^* \frac{\partial f(\eta, \tau^*)}{\partial \eta} (m-1) \right], \\ \tau^* &= \frac{bx^{m-1}}{(1 + Pr)^{2n}} t, \quad V_w = -\left(\frac{\alpha^*}{x} \right) \lambda \left[f_w \frac{m+1}{2} \right], \\ T &= (T_w - T_\infty) \theta(\eta, \tau^*) + T_\infty, \quad C = (C_w - C_\infty) \chi(\eta, \tau^*) + C_\infty \end{aligned} \right\} \tag{15}$$

By applying new self-similarity variable, Eqns. (12)-(14) can be expressed as

$$Pr \frac{\partial^3 f}{\partial \eta^3} \left(1 + \frac{1}{\beta_\tau} \right) + \left(\frac{m+1}{2} \right) f \frac{\partial^2 f}{\partial \eta^2} + m \left(1 + Pr \right)^{4n} - \left(\frac{\partial f}{\partial \eta} \right)^2 - \frac{\partial^2 f}{\partial \eta \partial \tau^*} = 0, \tag{16}$$

$$\frac{\partial^2 \theta}{\partial \eta^2} + \left(\frac{m+1}{2} \right) f \frac{\partial \theta}{\partial \eta} + Pr N_b \frac{\partial \theta}{\partial \eta} \frac{\partial \chi}{\partial \eta} + Pr N_t \left(\frac{\partial \theta}{\partial \eta} \right)^2 - \frac{\partial \theta}{\partial \tau^*} = 0, \tag{17}$$

$$\frac{\partial^2 \chi}{\partial \eta^2} + \left(\frac{m+1}{2} \right) f \frac{\partial \chi}{\partial \eta} \frac{Sc}{Pr} + \frac{N_T}{N_b} \frac{\partial^2 \theta}{\partial \eta^2} - \frac{\partial \chi}{\partial \tau^*} = 0. \tag{18}$$

and boundary conditions are

$$\begin{aligned} f(0, \tau^*) &= f_w, \quad f'(0, \tau^*) = \lambda_\tau (1 + Pr)^{2n}, \quad \theta(0, \tau^*) = 1, \quad \chi(0, \tau^*) = 1 \quad \text{at } \eta = 0, \\ f'(\eta, \tau^*) &\rightarrow (1 + Pr)^{2n}, \quad \theta(\eta, \tau^*) \rightarrow 0, \quad \chi(\eta, \tau^*) \rightarrow 0 \quad \text{as } \eta \rightarrow \infty. \end{aligned} \tag{19}$$

The stability test is performed by using the following perturbation expressions for the fluid transport equations $f = f_0(\eta)$, $\theta = \theta_0(\eta)$ and $\chi = \chi_0(\eta)$ with below conditions

$$\left. \begin{aligned} f(\eta, \tau^*) &= f_0(\eta) + e^{-\gamma \tau^*} F(\eta), \\ \theta(\eta, \tau^*) &= \theta_0(\eta) + e^{-\gamma \tau^*} S(\eta), \\ \chi(\eta, \tau^*) &= \chi_0(\eta) + e^{-\gamma \tau^*} P(\eta). \end{aligned} \right\} \tag{20}$$

where γ is an unidentified eigenvalue and $f_0(\eta)$, $\theta_0(\eta)$ and $\chi_0(\eta)$ are higher relative to $F(\eta)$, $S(\eta)$ and $P(\eta)$, respectively. The following system of equations is received by using Eqn. (20) into Eqns. (16)-(18):

$$Pr F''' \left(1 + \frac{1}{\beta_\tau} \right) + \left(\frac{m+1}{2} \right) (f_0 F'' + F f_0') - (2m f_0' - \gamma) F' = 0, \tag{21}$$

$$S'' + \left(\frac{m+1}{2} \right) (f_0 S' + F \theta_0') + Pr N_b \theta_0' P' + Pr S' (N_b \chi_0' + 2N_T \theta_0') + \gamma S = 0, \tag{22}$$



$$P'' + \left(\frac{m+1}{2}\right) \left(\frac{Sc}{Pr}\right) (f_0 P' + F\chi_0') + \frac{N_T}{N_B} S'' + \frac{Sc}{Pr} \gamma P = 0. \tag{23}$$

along with the boundary conditions

$$\begin{aligned} F(\eta) = 0, F'(\eta) = 0, S(\eta) = 0, P(\eta) = 0 & \quad \text{at } \eta = 0, \\ F'(\eta) = 0, S(\eta) \rightarrow 0, P(\eta) \rightarrow 0 & \quad \text{as } \eta \rightarrow \infty. \end{aligned} \tag{24}$$

Solving the eigenvalue problem numerically for specific values of $Pr = 1.2, \beta_T = 3, f_w = 1, Sc = 3, N_T = 0.1,$ and $N_B = 0.1,$ we have receive an infinite set $(\gamma_1 < \gamma_2 < \gamma_3 < \dots)$ of eigenvalues. If γ is positive, then the solution is stable, whereas if γ is negative, then the solution is unstable. Harris et al. [43] have stated that normalization of a suitable boundary condition on $F(\eta), S(\eta)$ or $P(\eta)$ is essential to find out the eigenvalues. In the present model, the condition $F'(\eta) \rightarrow 0$ as $\eta \rightarrow \infty$ is normalized and the new condition $F''(0) = 1$ is employed to solve flow equations.

4. Numerical Solution

Set of non-linear dimensionless Eqns. (7)-(9) with the corresponding boundary conditions Eqn. (10) are solved using bvp4c collocation formula in MATLAB and 10^{-6} is the level of error tolerance. Bvp4c is a MATLAB package that provides the solution using the 3-stage Lobatto IIIa formula and the finite difference scheme. Besides, suitable initial guesses are required to obtain a better solution. The procedures of this solver are clearly expressed in Shampine et al. [44]. To employ this method, it is important to convert higher-order ODEs into the first-order ODEs. For such a conversion, the following processes are utilized. below mentioned a new set of variables are employed for computation:

$$\begin{aligned} f = a_1, f' = a_2, f'' = a_3, f''' = a_3' \\ \theta = a_4, \theta' = a_5, \chi = a_6, \chi' = a_7 \end{aligned} \tag{25}$$

applying Eq. (25) in Eqns. (7)-(10), then the reduced ODE equations are:

$$\left. \begin{aligned} a_1' &= a_2, \\ a_2' &= a_3, \\ a_3' &= - \left[\frac{\left(\frac{m+1}{2}\right) a_1 a_3 + m \left((1+Pr)^{4n} - (a_2)^2 \right)}{Pr \left(1 + \frac{1}{\beta_T} \right)} \right], \\ a_4' &= a_5, \\ a_5' &= - \left[\left(\frac{m+1}{2}\right) a_1 a_5 + Pr N_B a_5 a_7 + Pr N_T (a_5)^2 \right], \\ a_6' &= a_7, \\ a_7' &= - \left[\left(\frac{m+1}{2}\right) a_1 a_7 \frac{Sc}{Pr} + \frac{N_T}{N_B} a_5' \right]. \end{aligned} \right\} \tag{26}$$

with conditions are

$$\left. \begin{aligned} a_1(\eta) = f_w, \\ a_2(\eta) = \lambda_T (1+Pr)^{2n}, \\ a_4(\eta) = 1, \\ a_6(\eta) = 1 \end{aligned} \right\} \quad \text{at } \eta = 0, \tag{27}$$

$$\left. \begin{aligned} a_2(\eta) = (1+Pr)^{2n}, \\ a_4(\eta) \rightarrow 0, \\ a_6(\eta) \rightarrow 0 \end{aligned} \right\} \quad \text{as } \eta \rightarrow \infty.$$

The first solution obtained on Nu' for various Casson fluid parameter values are compared with Maple (dsolve incorporated by the midpoint) which is illustrated in Table 1. It is seen that the present results and the Maple results are in good agreement.

5. Results and Discussion

The main objective of this section is to provide a graphical description of velocity, temperature, and concentration distribution with the impacts of active parameters in two different geometry cases. The dimensionless flow equations with suitable boundary conditions have been computed via bvp4c. It is noteworthy to mention that the transport properties are analyzed over a wedge ($\beta_1 = 0.5$) and stagnation point ($\beta_1 = 1.0$). Two solutions are obtained with the expanding/contracting wedge and stagnation point surfaces. Hence the prime intention is to find out the critical points corresponding to the emerging parameters in the two solutions. A stability test is carried out to check which of the two solutions is stable. Red and blue colors represent the Casson nanofluid characteristics over a permeable wedge and stagnation point cases, respectively. Further, the solid and dashed lines show the first and second solutions.



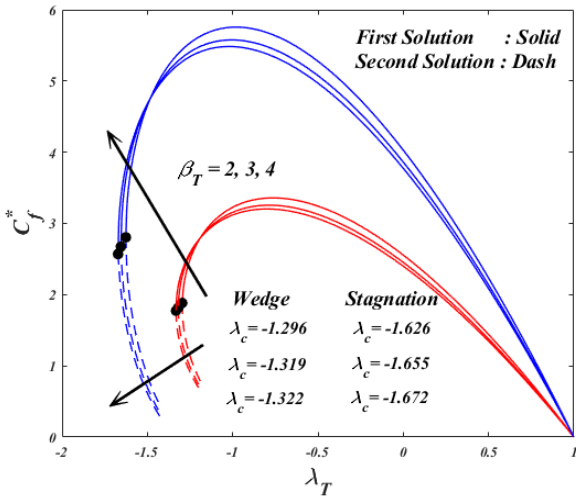


Fig. 2. Impacts of λ_T and β_T on C_f^*

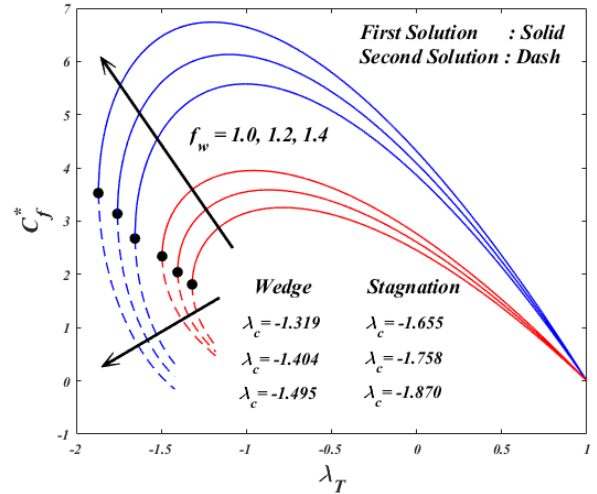


Fig. 3. Impacts of λ_T and f_w on C_f^*

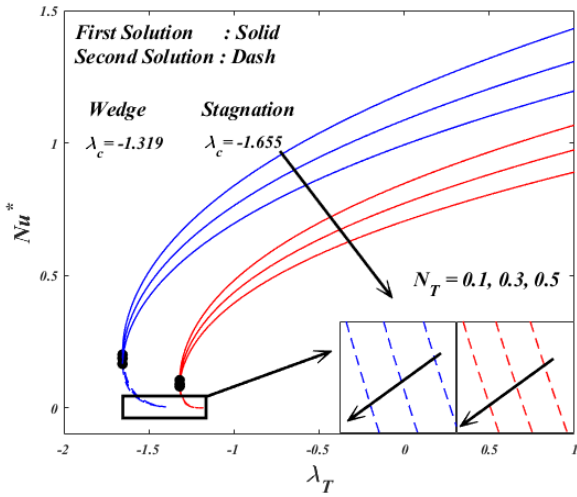


Fig. 4. Impacts of λ_T and N_T on Nu^*

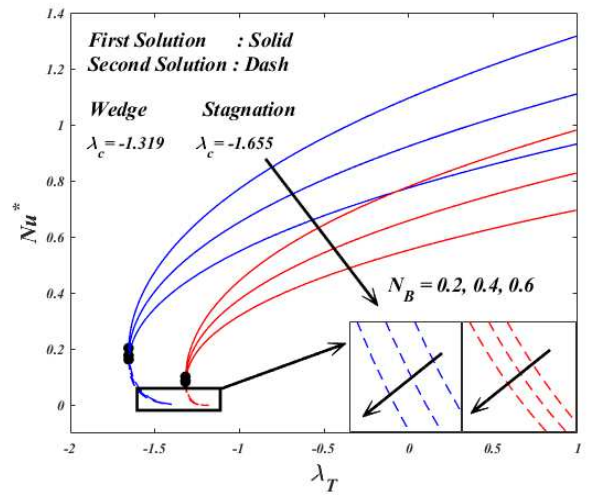


Fig. 5. Impacts of λ_T and N_B on Nu^*

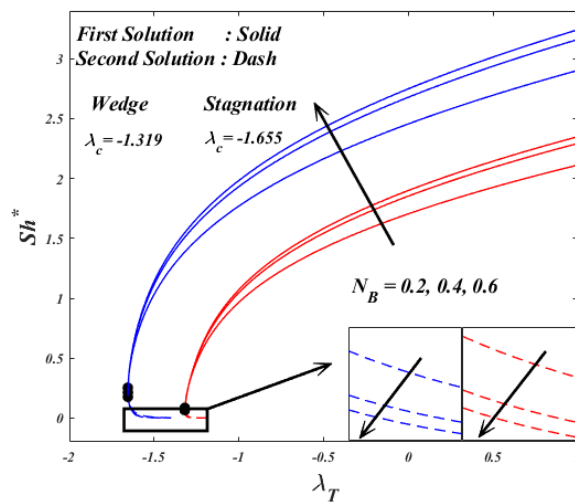


Fig. 6. Impacts of λ_T and N_B on Sh^*



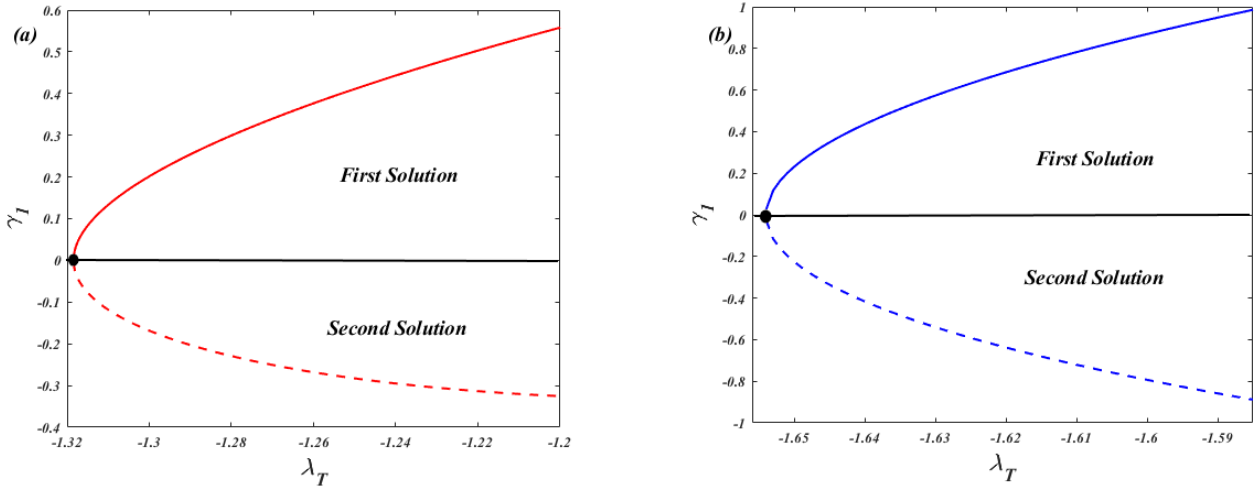


Fig. 7. (a,b) Plot of smallest eigenvalues for uplifting λ_T for (a) $\beta_1 = 0.5$ (b) $\beta_1 = 1$.

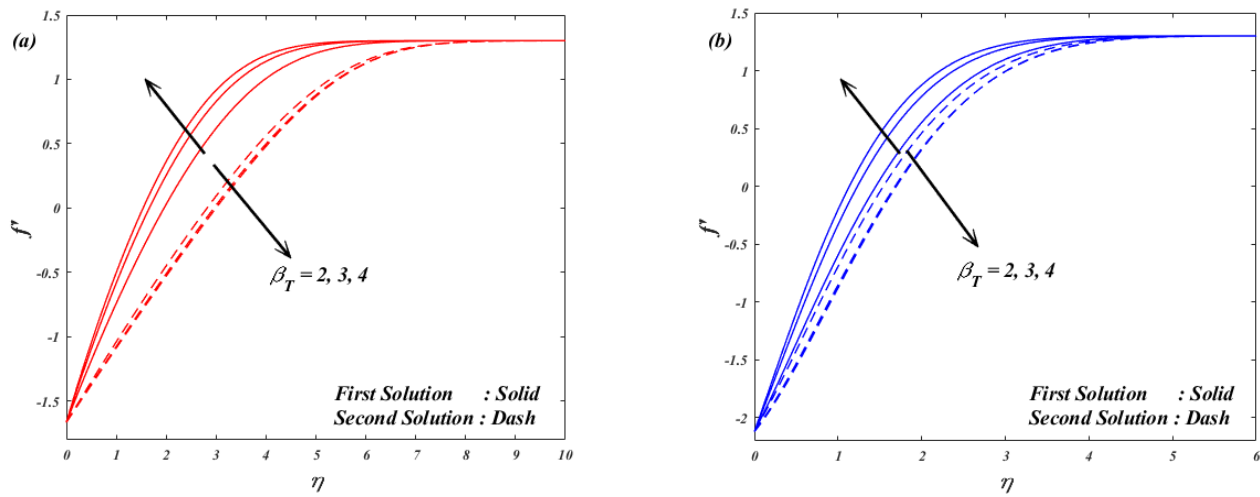


Fig. 8. (a,b) Plot of f' for uplifting β_T for (a) $\beta_1 = 0.5$ (b) $\beta_1 = 1$.

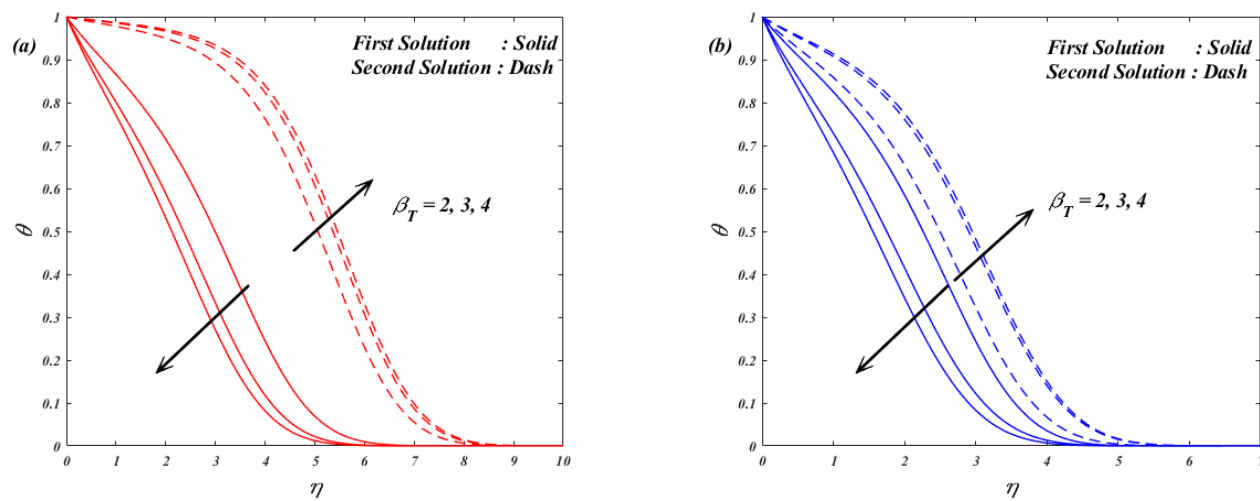


Fig. 9. (a,b) Plot of θ for uplifting β_T for (a) $\beta_1 = 0.5$ (b) $\beta_1 = 1$.



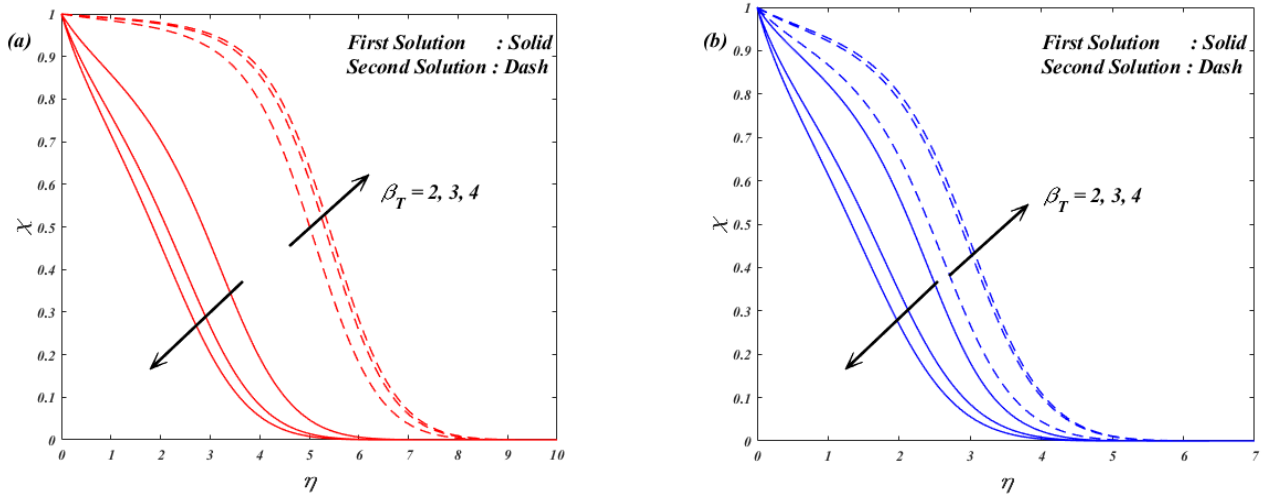


Fig. 10. (a,b) Plot of χ for uplifting β_T for (a) $\beta_1 = 0.5$ (b) $\beta_1 = 1$.

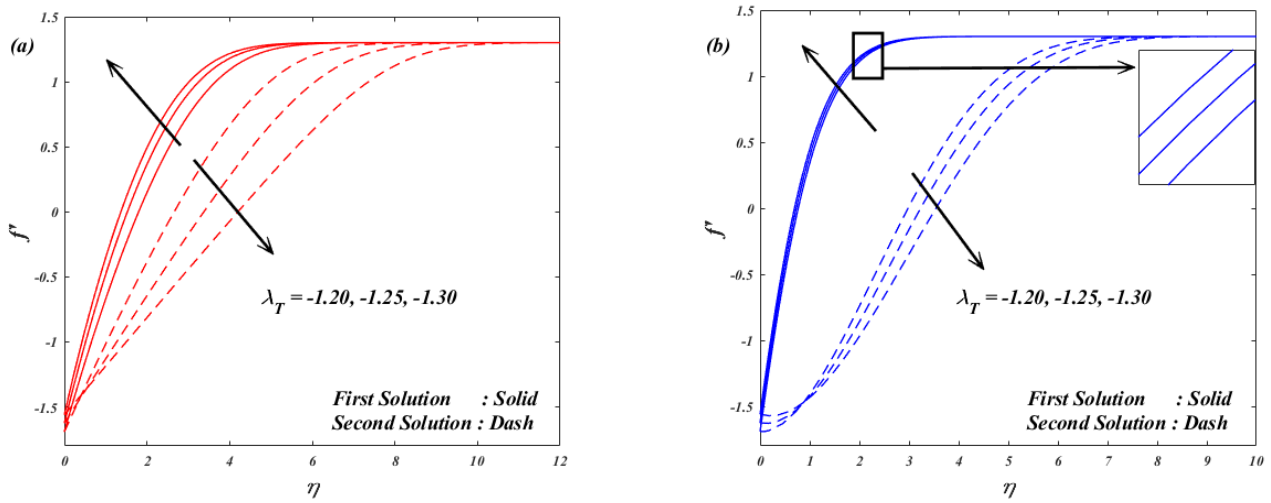


Fig. 11. (a,b) Plot of f' for uplifting λ_T for (a) $\beta_1 = 0.5$ (b) $\beta_1 = 1$.

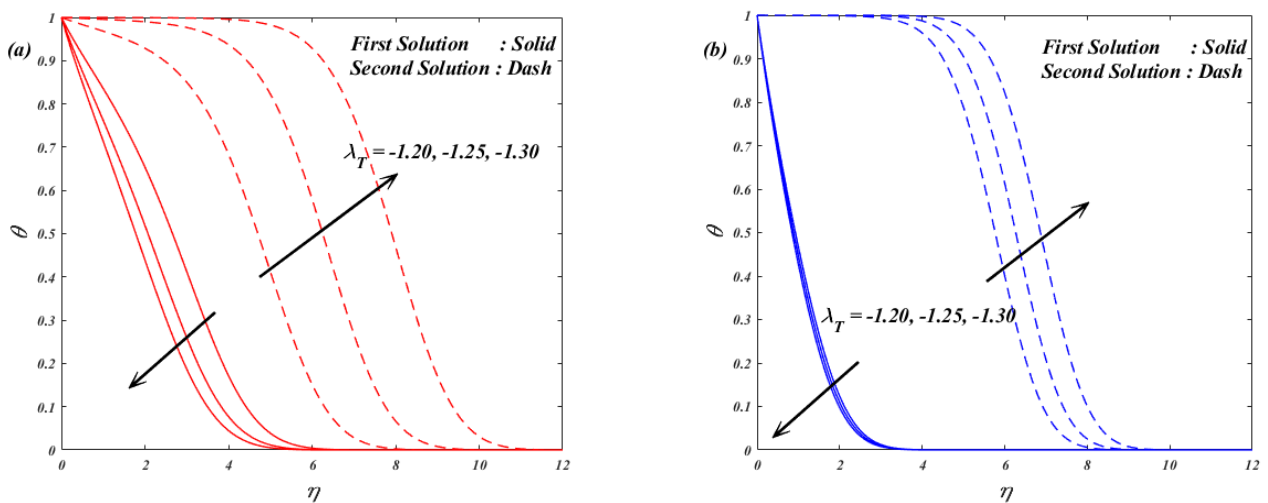


Fig. 12. (a,b) Plot of θ for uplifting λ_T for (a) $\beta_1 = 0.5$ (b) $\beta_1 = 1$.



Figures 2-6 elucidate the dual natures of Casson nanofluid for various values of λ_T over two different geometry cases. It is observed from these figures that first and second solutions exist for $\lambda_T > \lambda_c$ unique solution exists for $\lambda_T = \lambda_c$ and there is no solution for $\lambda_T < \lambda_c$, where lower script c expresses the critical value. Figure 2 discloses the impact of λ_T and β_T on C_f^* for two different geometry cases, respectively. It is observed from this figure that there are two solutions for $\lambda_c < \lambda_T < 0$ where the critical values of λ_T are $\lambda_c \approx -1.296, -1.319, -1.322$ for wedge case and $\lambda_c \approx -1.626, -1.655, -1.672$ for stagnation point case. Further, it noticed that the first solution enhances the skin friction at the surface whereas the reverse trend is seen for the second solution. Figure 3 accords the behavior of variation of C_f^* versus λ_T for higher values of f_w . In this figure, we have found that two solutions exist for a fixed value of λ_T when $\lambda_T \leq \lambda_c$. The critical values of λ_T are $\lambda_c \approx -1.319, -1.404, -1.495$ over the wedge and $\lambda_c \approx -1.655, -1.758, -1.870$ over the stagnation point for $f_w = 1, 1.2, 1.4$, respectively. Moreover, the first solution uplifts C_f^* by enhancing f_w whereas the second solution lessens the C_f^* at the surface.

Figure 4 manifests the influence of N_T and λ_T on Nu^* . This graph reveals that the first solution tends to decline Nu^* and the second solution tends to inflate Nu^* . The critical values of λ_T in order remain at $\lambda_c \approx 1.319$ and $\lambda_c \approx -1.655$ for the wedge and stagnation point with an upsurge value of N_T . Figure 5 exhibits the changes in Nu^* for several values of N_B and λ_T . It is evident from this figure that two solutions exist at the same critical value $\lambda_c \approx 1.319$ and $\lambda_c \approx -1.655$ of λ_T in wedge and stagnation point cases, respectively.

Changes in Sh^* due to N_B with λ_T are plotted in Fig. 6. It is important to note that this figure has the same critical points, $\lambda_c \approx 1.319$ and $\lambda_c \approx -1.655$, in cases of wedge and stagnation point for the given values of N_B . In addition, it is observed that both the solution augments Sh^* . Figure 7(a,b) is plotted to illustrate the positive and negative values of γ_1 for the first and second solutions. It is revealed that the first solution over two different geometries is stable while another solution is unstable.

The influence of varying β_T , on f', θ and χ is plotted in Figs. 8(a,b)-10(a,b) for $\beta_1 = 0.5$ and $\beta_1 = 1$ cases. Figure 8(a,b) illustrates that the uplifting values of β_T elevate f' . In permeable case, the buoyancy force controls the viscous force which tends to increase the velocity. Through Figs. 9(a,b) and 10(a,b), the changes in θ and χ are reported for higher values of β_T . Due to the influence of buoyancy force, the viscosity of the Casson nanofluid dissipates and manifests a decreasing behavior in temperature and concentration distributions for the first solution. The variation of λ_T on f' and θ are displayed in Figs. 11(a,b) and 12(a,b). Figure 11(a,b) portrays how λ_T affects f' . It is clear from this figure that the f' shows an increasing nature by improving the values of λ_T in the stable solution (first solution). In contrast, in the second solution, Casson nanofluid velocity expresses a decreasing behavior. Further, it is noticed that the momentum related boundary thickness is higher for the first solution compared with the second solution. Figure 12(a,b) depicts the effect of λ_T on θ . It is evident from the stable solution that the thermal related boundary layer thickness is inflating with the enhancing λ_T values while the opposite trend is observed for the second solution.

Figures 13(a,b) -15(a,b) are sketched to explore the influence of f_w on f', θ and χ . Figure 13(a,b) discloses the influence of f_w on f' . For the stable solution, it is observed that the Casson nanofluid velocity increases when injecting the fluid into the surface. Physically, enhancing the fluid injection used to increase the momentum related boundary layer thickness which augments the fluid flow near the surface but the opposite nature is observed for the second solution. Impact of f_w on θ is demonstrated in Fig. 14(a,b). It is clear that the higher values of f_w augment the Casson nanofluid temperature for the stable solution case and reduce the temperature for the second solution case. Further, it is to be noted that injecting the fluid at the surface leads to reduce the thermal related boundary layer thickness. As a result, the Casson nanofluid temperature decreases. Effect of f_w on χ is plotted in Fig. 15(a,b). Physically, when injecting fluid at the surface tends to diminish the mass related boundary layer thickness, hence χ declines. Figure 16(a,b) demonstrate the effect of N_T on θ . In the phenomenon of thermophoresis, the heated particles are pushed from the hot surfaces to the cold area, as a result, the thermal related boundary layer rises with an increase in N_T for both the solutions. The effect of N_B on Casson nanofluid temperature is exhibited in Fig. 17(a,b). From this figure, it is clear that the first and second solutions manifest an uplifting nature for elevating the Brownian movement. As the Brownian motion increases, the random motion of the fluid particles enhances which causes to generate more heat and hence the fluid temperature rises. Figures 18 and 19 are sketched to disclose the impact of Nu^* on λ_T against N_B over the wedge and stagnation point cases, respectively. These figures are plotted with 40×40 meshes of λ_T and N_B . In addition, over the wedge, λ_T has the same critical value $\lambda_c \approx -1.319$ and over the stagnation point the critical value is $\lambda_c \approx -1.655$. It is manifested that the first and second solutions have a reverse behavior on Nu^* for both $\beta_1 = 0.5$ and $\beta_1 = 1$.

6. Conclusion

This study aimed at exploring the dual natures and stability performance of Casson nanofluid over an extending/contracting wedge and stagnation point. Governing equations have been modeled by utilizing Buongiorno nanofluid model. The surface is permeable and suction/injection is considered. Two solutions are detected in a certain region when the wedge and stagnation point surface are extended/contracted. A depth stability test is performed which helps to examine the stability of the obtained solutions. The two-dimensional plot, three-dimensional surface plot and contour plot are used to exhibit the outcomes. The main findings of the current study are listed below.

- The first and second solutions have an opposite nature on the fluid velocity due to the impact of Casson fluid parameter.
- The Casson nanofluid temperature enhances with an increment in thermophoresis and Brownian motion for both the solutions.
- Skin friction factor augments at the surface for higher values of Casson fluid parameter and suction/injection in case of the first solution.
- Brownian motion has the same critical point on the rates of heat and mass transfer.
- The stagnation point case has higher rates of heat and mass transfer than wedge.
- From this model, it is evident that the first solution is stable and physically realizable.



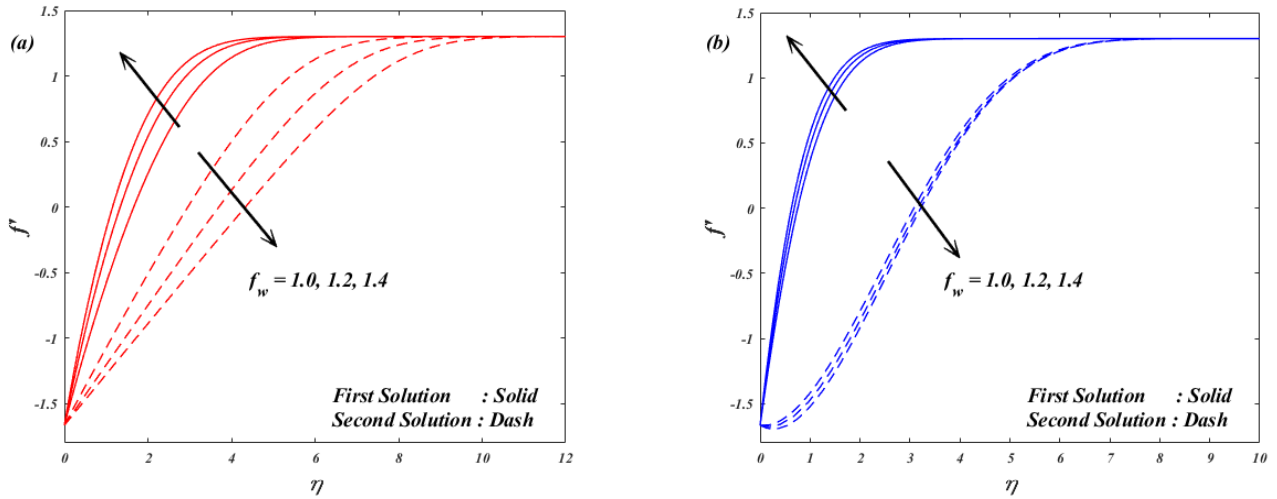


Fig. 13. (a,b) Plot of f' for uplifting f_w for (a) $\beta_1 = 0.5$ (b) $\beta_1 = 1$.

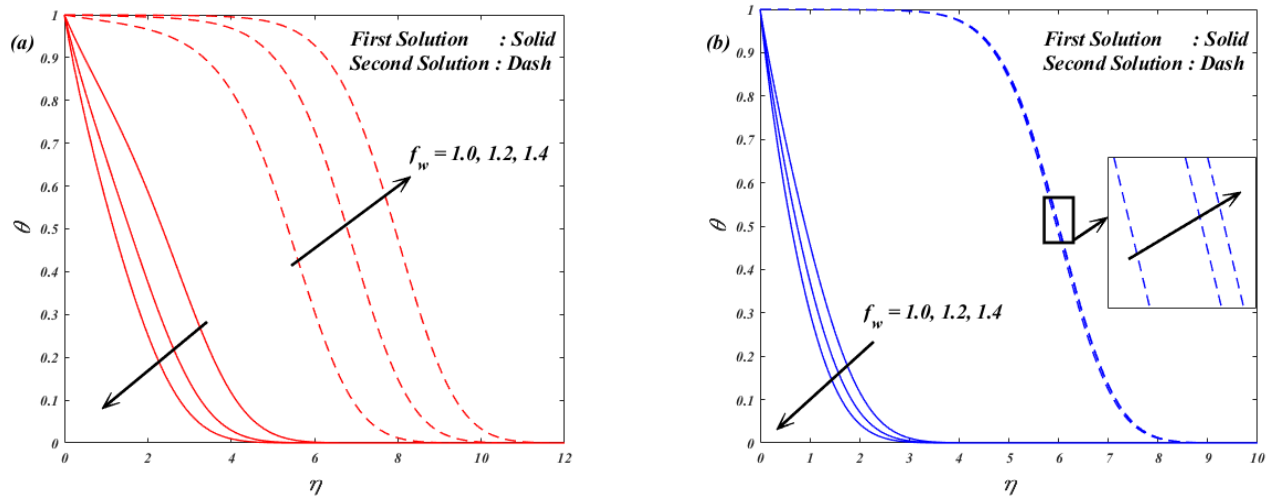


Fig. 14. (a,b) Plot of θ for uplifting f_w for (a) $\beta_1 = 0.5$ (b) $\beta_1 = 1$.

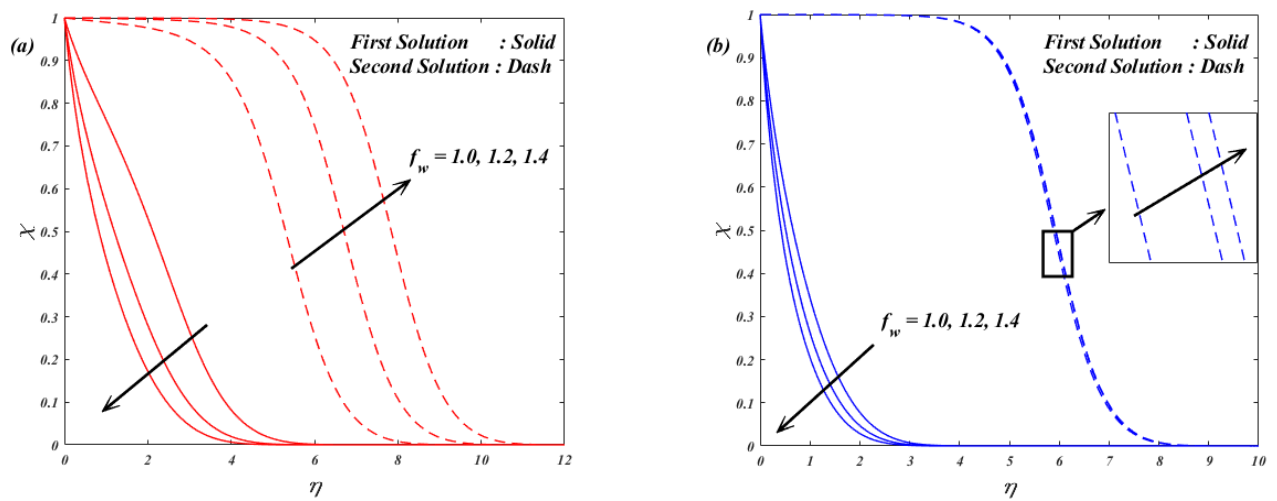


Fig. 15. (a,b) Plot of χ for uplifting f_w for (a) $\beta_1 = 0.5$ (b) $\beta_1 = 1$.



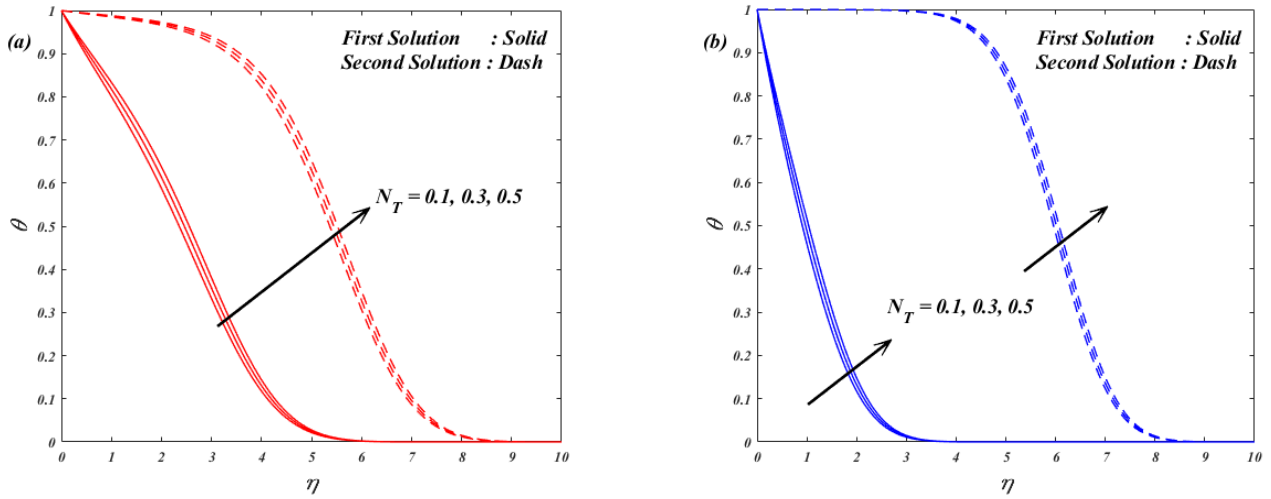


Fig. 16. (a,b) Plot of θ for uplifting N_T for (a) $\beta_1 = 0.5$ (b) $\beta_1 = 1$.

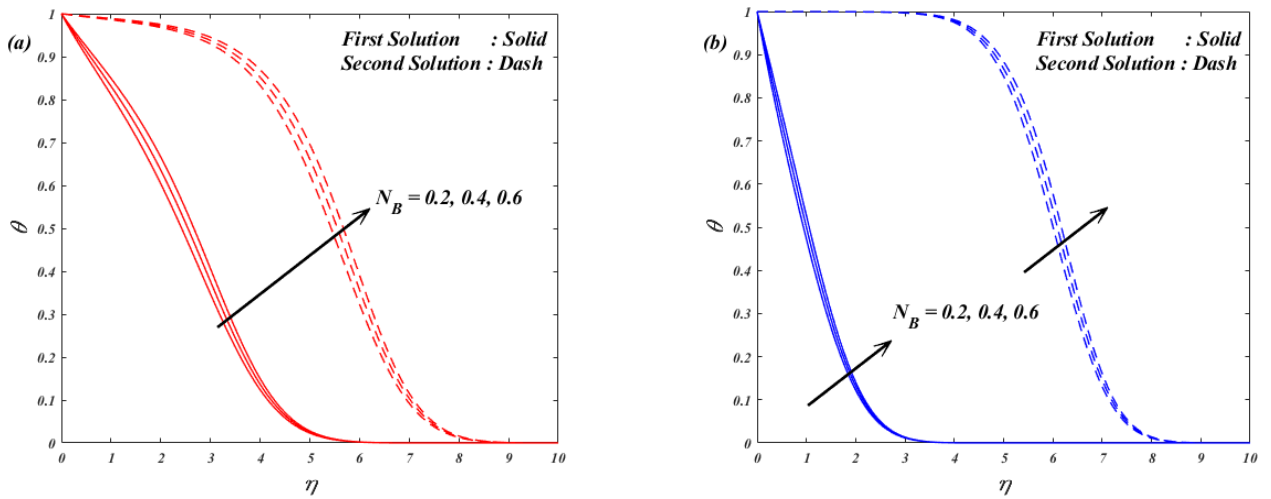


Fig. 17. (a,b) Plot of θ for uplifting N_B for (a) $\beta_1 = 0.5$ (b) $\beta_1 = 1$.

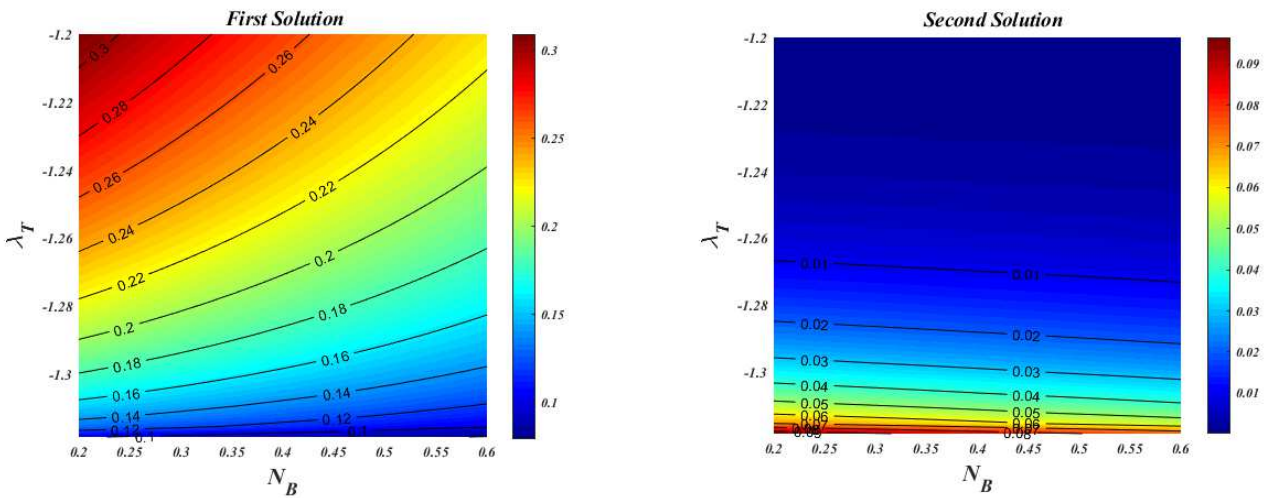


Fig. 18. Surface and contour plots with the effects of N_B and λ_T on Nu' for two solutions when $\beta_1 = 0.5$.



Table 1. Comparison of the values of β_r on Nu' with Maple (dsolve) for first solution

Parameter	Nu'			
	First solution			
	wedge		Stagnation point	
β_r	bvp4c	dsolve	bvp4c	dsolve
	MATLAB	Maple	MATLAB	Maple
2	0.157390	0.157395	0.647996	0.647990
3	0.231779	0.231771	0.686871	0.686869
4	0.266488	0.266492	0.707541	0.707543
5	0.286966	0.286969	0.720396	0.720400
6	0.300534	0.300539	0.729172	0.729176

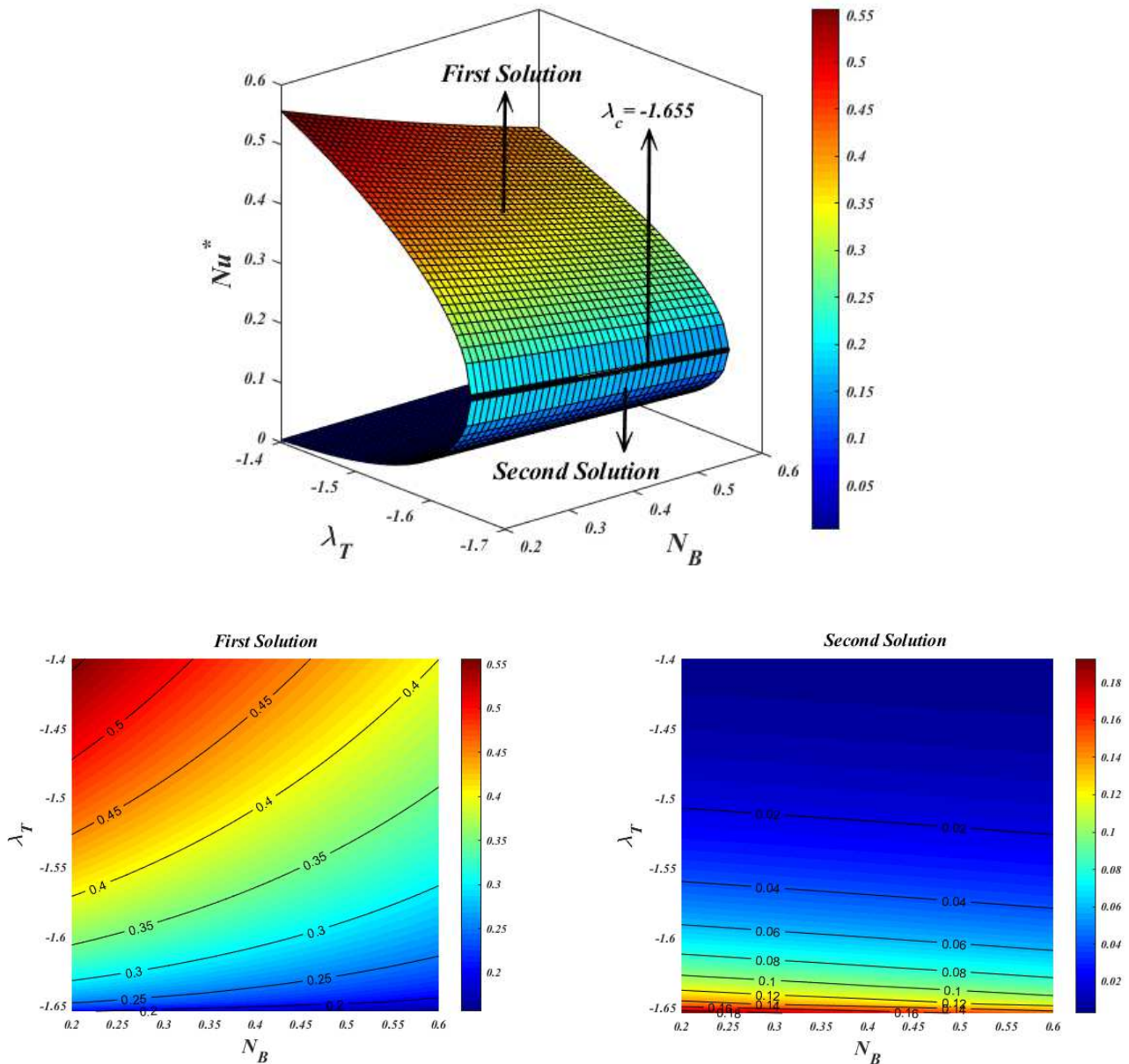


Fig. 19. Surface and contour plots with the effects of N_b and λ_T on Nu' for two solutions when $\beta_1 = 1.0$.

Author Contributions

H. Thameem Basha has formulated the mathematical model, solved numerically, and written the manuscript. R. Sivaraj has verified the mathematical model, solution procedure, numerical results, and improved the manuscript writing.

Acknowledgments

Not applicable.



Conflict of Interest

The authors declare that there is no conflict of interest.

Funding

The authors received no financial support for the research, authorship, and publication of this article.

Data Availability Statements

The datasets generated and/or analyzed during the current study are available from the corresponding author on reasonable request.

References

- [1] Sivaraj, R., Kumar, B.R., Unsteady MHD dusty viscoelastic fluid Couette flow in an irregular channel with varying mass diffusion, *International Journal of Heat and Mass Transfer*, 55, 2012, 3076–3089
- [2] Kumar, B.R., Sivaraj, R., Heat and mass transfer in MHD viscoelastic fluid flow over a vertical cone and flat plate with variable viscosity, *International Journal of Heat and Mass Transfer*, 56, 2013, 370–379.
- [3] Benazir, A.J., Sivaraj, R., Rashidi, M.M., Comparison Between Casson Fluid Flow in the Presence of Heat and Mass Transfer From a Vertical Cone and Flat Plate, *Journal of Heat Transfer*, 138, 2016, 112005.
- [4] Khan, W.A., Sultan, F., Ali, M., Shahzad, M., Khan, M., Irfan, M., Consequences of activation energy and binary chemical reaction for 3D flow of Cross - nanofluid with radiative heat transfer, *Journal of the Brazilian Society of Mechanical Sciences*, 41, 2019, 4.
- [5] Ali, L., Omar, Z., Khan, I., Analysis of dual solution for MHD flow of Williamson fluid with slippage, *Heliyon*, 5, 2019, e01345.
- [6] Casson, N., *A flow equation for the pigment oil suspensions of the printing ink type*, *Rheology of Disperse Systems*, Pergamon, New York, 1959, 84-102.
- [7] Mythili, D., Sivaraj, R., Influence of higher order chemical reaction and non-uniform heat source / sink on Casson fluid flow over a vertical cone and flat plate, *Journal of Molecular Liquids*, 216, 2016, 466–475.
- [8] Raju, C.S.K., Hoque, M.M., Sivasankar, T., Radiative flow of Casson fluid over a moving wedge filled with gyrotactic microorganisms, *Advanced Powder Technology*, 28, 2016, 575–583.
- [9] Hamid, M., Usman, M., Khan, Z.H., Ahmad, R., Wang, W., Dual solutions and stability analysis of flow and heat transfer of Casson fluid over a stretching sheet, *Physics Letters A*, 383, 2019, 2400–2408.
- [10] Rafique, K., Anwar, M.I., Misiran, M., Khan, I., Alharbi, O., Thounthong P., Nisar K.S., Numerical Solution of Casson Nanofluid Flow Over a Non-linear Inclined Surface With Soret and Dufour Effects by Keller-Box Method, *Frontiers in Physics*, 11, 2019, 7.
- [11] Rafique, K., Anwar, M.I., Misiran, M., Khan, I., Alharbi, O., Thounthong P., Nisar K.S., Keller-Box Analysis of Buongiorno Model with Brownian and Thermophoretic Diffusion for Casson Nanofluid over an Inclined Surface, *Symmetry*, 11, 2019, 1370.
- [12] Ullah, I., Nisar K.S., Shafie, S., Khan, I., Qasim, M., Khan A., Unsteady Free Convection Flow of Casson Nanofluid Over a Nonlinear Stretching Sheet, *IEEE Access*, 7, 2019, 93076-93087.
- [13] Choi, S.U.S., Eastman, J.A., Enhancing thermal conductivity of fluids with nanoparticles, in Proceedings of the 1995 ASME International Mechanical Engineering Congress and Exposition, San Francisco, California, 1217 November (American Society of Mechanical Engineers, Fluids Engineering Division (Publication) FED, 1995), 231, 1995, 99-105.
- [14] Basha, H.T., Sivaraj, R., Reddy, A.S., Chamkha, A.J., SWCNH/diamond-ethylene glycol nanofluid flow over a wedge, plate and stagnation point with induced magnetic field and nonlinear radiation – solar energy application, *The European Physical Journal Special Topics*, 228, 2019, 2531–2551.
- [15] Hatami, M., Hatami, J., Ganji, D.D., Computer simulation of MHD blood conveying gold nanoparticles as a third grade non-Newtonian nanofluid in a hollow porous vessel, *Comput. Methods Programs Biomed.*, 113, 2013, 632–641.
- [16] Said, Z., Assad, M.E.H., Hachicha, A.A., Bellos, E., Ali, M., Zeyad, D., Yousef, B.A.A., Enhancing the performance of automotive radiators using nano fluids, *Renewable and Sustainable Energy Reviews*, 112, 2019, 183–194.
- [17] Ali F., Ali F., Sheikh, N.A., Khan, I., Nisar K.S., Caputo-Fabrizio fractional derivatives modeling of transient MHD Brinkman nanoliquid: Applications in food technology, *Chaos, Solitons & Fractals*, 131, 2020, 109489.
- [18] Abbasi F. M., Shanakhat I., Shehzad S. A., Analysis of entropy generation in peristaltic nanofluid flow with Ohmic heating and Hall current, *Physica Scripta*, 94, 2018, 025001.
- [19] Abbasi F. M., Shanakhat I., Shehzad S. A., Entropy generation analysis for peristalsis of nanofluid with temperature dependent viscosity and Hall effects, *Journal of Magnetism and Magnetic Materials*, 474, 2019, 434-441.
- [20] Buongiorno, J., Convective Transport in Nanofluids, *Journal of Heat Transfer*, 128, 2006, 240.
- [21] Basha, H.T., Sivaraj, R., Animasaun, I.L., Makinde, O.D., Influence of Non-Uniform Heat Source/Sink on Unsteady Chemically Reacting Nanofluid Flow over a Cone and Plate, *Defect and Diffusion Forum*, 389, 2018, 50–59.
- [22] Abbasi F. M., Shanakhat I., Shehzad S. A., Hall effects on peristalsis of boron nitride-ethylene glycol nanofluid with temperature dependent thermal conductivity, *Physica E: Low-dimensional Systems and Nanostructures*, 99, 2018, 275-284.
- [23] Waqas M., Shehzad S.A., Hayat T., Khan M. I., Alsaedi A., Simulation of magnetohydrodynamics and radiative heat transport in convectively heated stratified flow of Jeffrey nanofluid, *Journal of Physics and Chemistry of Solids*, 133, 2019, 45-51.
- [24] Riaz, A., Gul, A., Khan, I., Ramesh K., Khan, S.U., Baleanu, D., Nisar K.S., Mathematical Analysis of Entropy Generation in the Flow of Viscoelastic Nanofluid through an Annular Region of Two Asymmetric Annuli Having Flexible Surfaces, *Coatings*, 10, 2020, 213.
- [25] Basha, H.T., Sivaraj, R., Reddy, A.S., Chamkha A.J., Tilioua, M., Impacts of temperature-dependent viscosity and variable Prandtl number on forced convective Falkner-Skan flow of Williamson nanofluid, *SN Applied Sciences*, 2, 2020, 477.
- [26] Zaimi K., Ishak A., Pop I., Boundary layer flow and heat transfer over a nonlinearly permeable stretching/shrinking sheet in a nanofluid, *Scientific Reports*, 4, 2014, 4404.
- [27] Hamid R. A., Nazar R., Pop I., Non-alignment stagnation-point flow of a nanofluid past a permeable stretching/shrinking sheet: Buongiorno's model, *Scientific Reports*, 5, 2015, 14640.
- [28] Lu D., Ramzan M., Huda N., Chung J.D., Farooq U., Nonlinear radiation effect on MHD Carreau nanofluid flow over a radially stretching surface with zero mass flux at the surface, *Scientific Reports*, 8, 2018, 3709.
- [29] Khan N.S., Shah Q., Bhaumik A., Kumam P., Thounthong P., Amiri I., Entropy generation in bioconvection nanofluid flow between two stretchable rotating disks, *Scientific Reports*, 10, 2020, 4448.
- [30] Khan N.S., Kumam P., Thounthong P., Second law analysis with effects of Arrhenius activation energy and binary chemical reaction on nanofluid flow, *Scientific Reports*, 10, 2020, 1226.
- [31] Bachok, N., Ishak A., Pop, I., Melting heat transfer in boundary layer stagnation-point flow towards a stretching / shrinking sheet, *Physics Letters A*, 374, 2010, 4075–4079.
- [32] Alam, M.S., Khatun, M.A., Rahman, M.M., Vajravelu, K., Effects of variable fluid properties and thermophoresis on unsteady forced convective boundary layer flow along a permeable stretching / shrinking wedge with variable Prandtl and Schmidt numbers, *International Journal of Mechanical Sciences*, 105, 2016, 191–205.
- [33] Pop, I., Naganthran, K., Nazar, R. Numerical solutions of non-alignment stagnation-point flow and heat transfer over a stretching/shrinking surface in a nanofluid, *International Journal of Numerical Methods for Heat & Fluid Flow*, 26, 2016, 1747-1767.
- [34] Dogonchi, A.S., Ganji, D.D., Investigation of MHD nano fluid flow and heat transfer in a stretching / shrinking convergent / divergent channel considering thermal radiation, *Journal of Molecular Liquids*, 220, 2016, 592–603.
- [35] Hamid, A., Khan, M., Hafeez, A., Unsteady stagnation-point flow of Williamson fluid generated by stretching / shrinking sheet with Ohmic heating, *International Journal of Heat and Mass Transfer*, 126, 2018, 933–940.



- [36] Hashim, Khan, M., Khan, U., Stability analysis in the transient flow of Carreau fluid with non-linear radiative heat transfer and nanomaterials: Critical points, *Journal of Molecular Liquids*, 272, 2018, 787–800.
- [37] Usama, Nadeem, S., Khan, A.U., Stability analysis of Cu – H₂O nanofluid over a curved stretching / shrinking sheet: Existence of dual solutions, *Canadian Journal of Physics*, 97, 2019, 911–922.
- [38] Makinde, O.D., Stagnation Point Flow with Heat Transfer and Temporal Stability of Ferrofluid Past a Permeable Stretching/Shrinking Sheet, *Defect and Diffusion Forum*, 387, 2018, 510–522.
- [39] Ghadikolaei, S.S., Hosseinzadeh, K., Ganji, D.D., Investigation on Magneto Eyring-Powell nano fluid flow over inclined stretching cylinder with nonlinear thermal radiation and Joule heating effect, *World Journal of Engineering*, 16, 2019, 51–63.
- [40] Khan, U., Ahmad, S., Hayyat, A., Khan, I., Nisar, K. S., Baleanu, D., On the Cattaneo–Christov Heat Flux Model and OHAM Analysis for Three Different Types of Nanofluids, *Applied Sciences*, 10, 2020, 886.
- [41] Lin, H.T., Lin, L.K., Similarity solutions for laminar forced convection heat transfer from wedges to fluids of any Prandtl number, *International Journal of Heat and Mass Transfer*, 30, 1987, 1111–1118.
- [42] Makinde, O.D., On the Chebyshev collocation spectral approach to stability of fluid flow in a porous medium, *International Journal for Numerical Methods in Fluids*, 59, 2009, 791–799.
- [43] Harris, S.D., Ingham, D.B., Pop, I., Mixed Convection Boundary-Layer Flow near the Stagnation Point on a Vertical Surface in a Porous Medium: Brinkman Model with Slip, *Transport in Porous Media*, 77, 2009, 267–285.
- [44] Shampine, L.F., Gladwell, I., Thompson, S., *Solving ODEs with MATLAB*, Cambridge University Press, Cambridge, 2003.

ORCID iD

H.T. Basha  <http://orcid.org/0000-0002-2016-5086>

R. Sivaraj  <http://orcid.org/0000-0002-0841-3948>



© 2022 Shahid Chamran University of Ahvaz, Ahvaz, Iran. This article is an open access article distributed under the terms and conditions of the Creative Commons Attribution-Noncommercial 4.0 International (CC BY-NC 4.0 license) (<http://creativecommons.org/licenses/by-nc/4.0/>).

How to cite this article: Basha H.T., Sivaraj R. Stability Analysis of Casson Nanofluid Flow over an Extending/Contracting Wedge and Stagnation Point, *J. Appl. Comput. Mech.*, 8(2), 2022, 566–579. <https://doi.org/10.22055/JACM.2020.32618.2045>

Publisher's Note Shahid Chamran University of Ahvaz remains neutral with regard to jurisdictional claims in published maps and institutional affiliations.

